Biointerface Laboratory at Helmholtz-Institute for Biomedical Engineering

RWTH AACHEN UNIVERSITY

Faculty of Medicine

Cell-Material Interactions: Translating Basic Science Into Clinical Applications

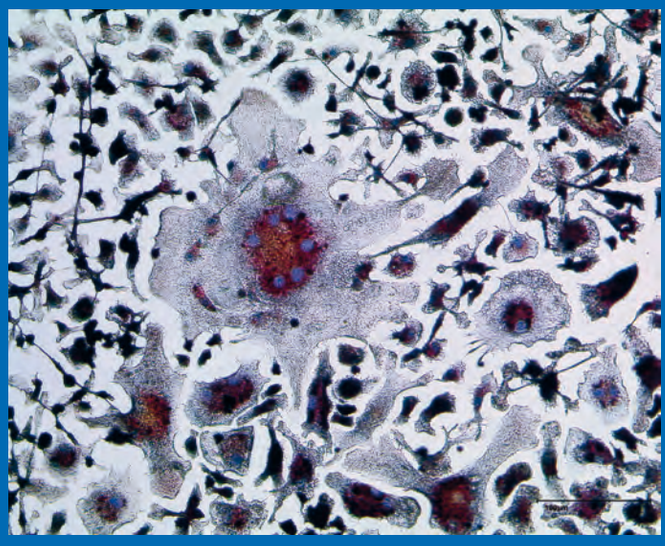

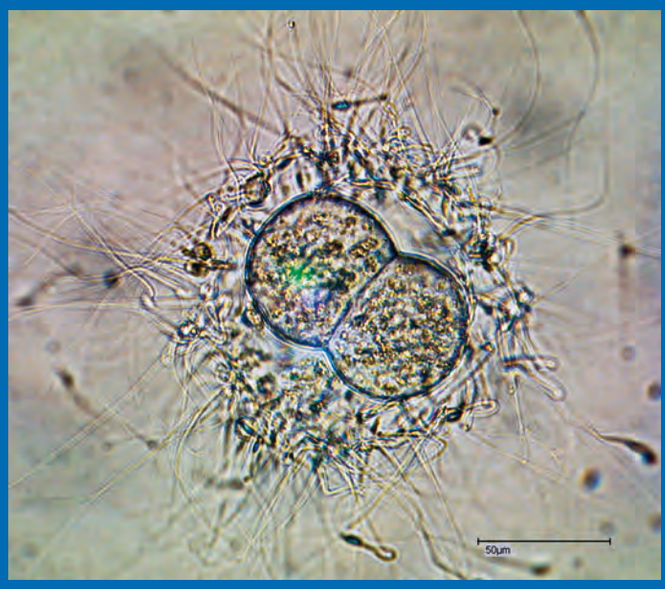

Director

Univ.-Prof. Dr. rer. nat.
Wilhelm Jahnen-Dechent

RWTH Aachen University Hospital
Pauwelsstrasse 30, 52074 Aachen

Helmholtz-Institute for Biomedical Engineering
Pauwelsstrasse 20, 52074 Aachen

Phone: +49 (0)241 80-80157 (Secretary)
+49 (0)241 80-80163 (Office)
Fax: +49 (0)241 80-82573
Email: rsous@ukaachen.de
Web: http://www.biointerface.rwth-aachen.de

Staff

Sous, Renate Administrative Assistant
Bienert, Michaela Dr. rer. nat.
Bruhns, Florian
Büscher, Andrea MSc
Dzhanaev, Robert
Floehr, Julia Dr. rer. nat.
Gräber, Steffen CTA
Jung, Nadine BSc
Köppert, Sina Ing. MSc
Labude, Norina MTA
Malayran, Hanna BSc
Neidig, Kathrin BSc
Neuß-Stein, Sabine Prof. Dr. rer. nat.
Nowotny, Viola Cand Med
Peglow, Sarah BSc
Römer, Simon Cand Med
Sadr, Seyedeh Zeynab MSc
Schmitz, Carlo MSc
Schwarz, Miriam Cand Med
Sundararaman, Sai BSc
Tiefes, Marc BSc
Wein, Svenja MSc
Winkler, Camilla BSc
Wosnitza, Elisabeth BSc
Zenner, Laura BSc

Cover Figures: *Top, large osteoclast-like cells with several cell nuclei differentiated from monocytic cells in culture. Osteoclasts mediate bone resorption. They may also be instructed to resorb calcifications. To this end they must be locally activated with the targeted cytokines. Bottom, Two-Cell embryo developed entirely outside the body. Immature oocytes were harvested from early follicles, matured, and fertilized in cell culture dishes. The cleavage of fertilized oocytes is living proof of favorable culture conditions. In vitro maturation and fertilization become a necessity, if oocytes cannot be naturally fertilized for medical reasons.*

Introduction

In this past year we continued our highly collaborative research on the biological role of fetuin family proteins [1-6]. In what follows, additional work will be presented by the people who actually did the work.

Mammalian Plasma Fetuin-B is a Selective Inhibitor of Ovastacin and Meprin Metalloproteinases

MSc Carlo Schmitz
Dr. Julia Floehr

Mammalian fetuin-A and fetuin-B are circulating hepatic glycoproteins of the cystatin-superfamily of cysteine proteinase inhibitors. Both fetuin proteins belong to type III cystatins and consist of two successive cystatin-like domains followed by a C-terminal region. While fetuin-A is a potent inhibitor of ectopic calcification, fetuin-B was identified as a potent and specific inhibitor of the zinc metalloproteinase ovastacin and plays an essential role in oocyte fertilization.

In cooperation with the group of Prof. Walter Stöcker (Johannes Gutenberg University Mainz) and Prof. Ralf Weiskirchen (RWTH Aachen University) fetuin proteins were produced in baculovirus transduced High Five insect cells, adenovirus transduced Cos-7 cells and in plasmid transfected CHO cells. Molecular masses of recombinant proteins varied according to their degree of N-linked glycosylation (Fig. 1A). Glycan analysis revealed that Cos-7 and CHO cell-derived proteins had complex glycosylation with and without terminal sialic acid, while High Five insect cell products typically had mannose-terminated N-glycans resulting in a lower molecular weight. To evaluate the effect of glycosylation on fetuin-B activity, fetuin-B was also expressed in the presence of tunicamycin, which prevents regular glycosylation. Also, the proteins were produced in glycosylation deficient CHO Lec 3.2.8.1 cells. Regardless of the cells employed for recombinant protein production, fetuin-B strongly inhibited ovastacin activity, indicating that neither glycosylation nor the expression system affected fetuin-B activity (Fig. 1B).

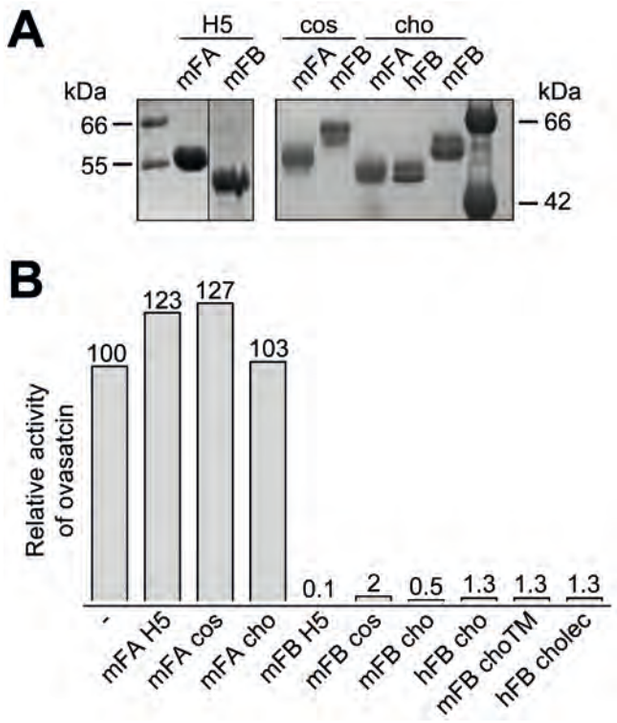

Fig. 1: Varying protein expression system does not alter inhibitory potency of fetuin-B.
(A) Recombinant fetuin-A and fetuin-B variants from human (hFB) and mouse (mFA, mFB) expressed in adenovirus transduced Cos-7 cells (cos), baculovirus infected High Five insect cells (H5) and plasmid transfected chinese hamster ovary cells (cho) were analyzed by SDS-PAGE followed by Coomassie staining. Molecular weight is indicated at both sides. (B) Inhibition of ovastacin by recombinant fetuin-B independent of the protein expression system. Glycosylation deficient CHO Lec 3.2.8.1 cells (cholec) were used to produce hFB; mFB was expressed in presence of tunicamycin (choTM) inhibiting N-glycosylation. The activity of ovastacin without additives was set to 100%.

Fetuin-B was the first known natural protein inhibitor of ovastacin, and is the first mammalian plasma protein that acts as a highly specific inhibitor of astacin metalloproteinases. We asked if further physiological target proteinases for fetuin-B exist. To this end we tested the inhibitory potential of fetuin-B against various metalloproteinases and cystein proteinases (Fig. 2).

Recombinant mouse fetuin-B inhibited mammalian astacin metalloproteinases meprin α and meprin β with similar potency like it inhibited ovastacin. Additionally, there was potent inhibition of non-mammalian astacins such as zebrafish nephrosin and crayfish astacin. Astacin family members tolloid-like protein 2 (TLL2) and bone morphogenetic protein-1 (BMP1) as well as various matrix metalloproteinases (MMPs) and cysteine proteinases were not inhibited by fetuin-B. Un-

like fetuin-B, fetuin-A did not inhibit any of the proteinases tested. While the regulated inhibition of ovastacin by fetuin-B is essential to maintain female fertility, the consequences of fetuin-B inhibition of meprin proteinases are less well understood. Meprins are pivotal in proteolytic networks controlling angiogenesis, immune defense, extracellular matrix assembly and general cell signaling. and therefor fetuin-B inhibition of these enzymes may affect many physiological pathways.

Class	Proteinase	fetuin-A K_i [nM]; IC_{50} [nM]	fetuin-B K_i [nM]; IC_{50} [nM]
Metalloproteinases	meprin α	n.i.	K_i 7±0.8
	meprin β	n.i.	K_i 33±2.4
	astacin	n.i.	K_i 16±1.5
	ovastacin	n.i.	IC_{50} 18±1.2
	nephrosin	n.i.	IC_{50} 0.6±0.1
	TLL2	n.i.	n.i.
	BMP1	n.i.	n.i.
	MMP-2/8/9/13	n.i.	n.i.
Cysteine proteinases	legumain	n.i.	n.i.
	papain	n.i.	n.i.
	cathepsin B/K/S	n.i.	n.i.

Fig. 2: Inhibition of proteinases by recombinant mouse fetuin-A and fetuin-B.
Proteinase activity assays were performed with fluorescent substrates. Due to detection limits of substrate hydrolysis at low enzyme concentrations, it was not possible to determine a Ki-value for ovastacin and nephrosin. Instead IC_{50} was calculated. n.i.: no inhibition.

Cellular Clearance and Biological Activity of Calciprotein Particles Depend on their Maturation State and Crystallinity


Ing. MSc Sina Köppert, MSc Andrea Büscher

The liver-derived plasma protein fetuin-A is a systemic inhibitor of ectopic calcification. Fetuin-A stabilizes saturated mineral solutions by forming colloidal protein-mineral complexes called calciprotein particles (CPP). CPP are initially spherical, amorphous and soft, and are referred to as primary CPP. These particles spontaneously convert into secondary CPP, which are larger and more crystalline. CPP mediate excess mineral transport and clearance from circulation.

We studied by intravital two-photon microscopy the clearance of primary vs. secondary CPP by injecting fluorescent CPP in mice. We analyzed CPP organ distribution and identified CPP endocytosing cells by immunofluorescence. Primary and secondary CPP were taken up by liver and spleen, but do not co-localize (Fig. 3 A, B). Only primary CPP were rapidly cleared by liver sinusoidal endothelial cells (LSEC) (Fig. 3 D), whereas primary and secondary CPP were cleared by Kupffer cells (Fig. 1 C, E). Cellular clearance was further studied using bone marrow-derived mouse wildtype and scavenger receptor A (SRA)-deficient macrophages, as well as human umbilical cord endothelial cells (HUVEC). Scavenger receptor A (SRA)-deficient bone marrow macrophages endocytosed secondary CPP less well than did wildtype macrophages. In contrast, primary CPP endocytosis did not depend on the presence of SRA, suggesting involvement of an alternative clearance pathway. We employed mouse wildtype and mutant immortalized macrophages to analyze CPP-induced inflammasome activation and cytokine secretion.

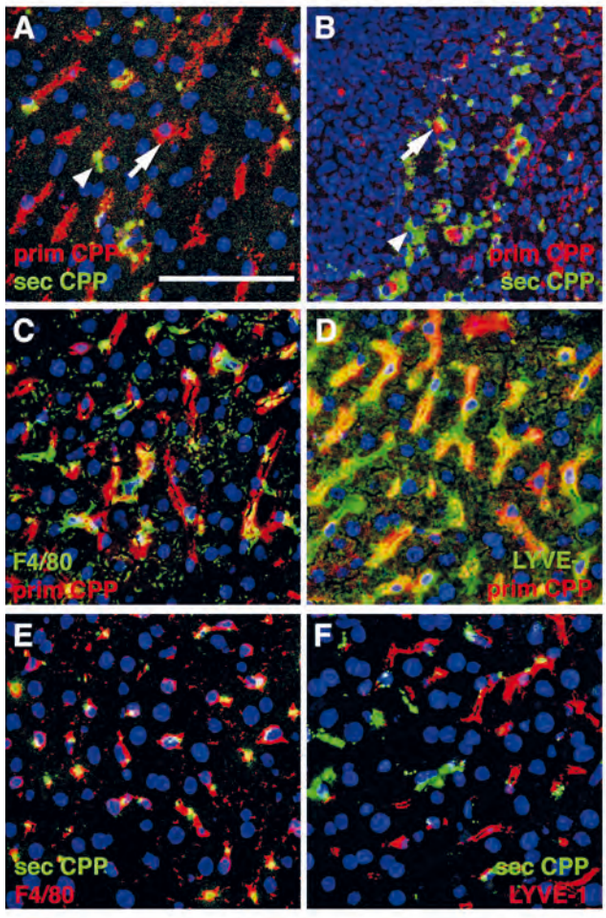

Fig. 3: Differential clearance of primary and secondary CPP.
Mice were injected with fluorescence labeled primary (red) and secondary CPP (green) and the major clearance organs liver (A, C-F) and spleen (B) were analysed for the presence of CPP, 10 minutes after injection. Primary CPP (prim CPP, arrows in A, B) and secondary CPP (sec CPP, arrow heads in A, B) showed distinct non-overlapping distribution in liver (A), and spleen (B). C-F, Co-localization with the macrophage-specific marker F4/80 and the liver sinusoidal endothelial LSEC-specific marker LYVE-1 suggested that primary CPP were predominantly cleared by LYVE-1-positive LSEC, and secondary CPP by F4/80-positive liver Kupffer cell macrophages. Scale bar: 25 µm. Figure taken from ref [8].

Figure 4 shows that CPP triggered TLR4 dependent TNF α and IL-1β secretion in cultured macrophages. Primary CPP treatment of macrophages caused low level TNFα secretion, yet strong IL-1β secretion. Primary CPP caused twice more IL-1β secretion than did secondary CPP (Fig. 4 C, D), which was associated with increased calcium-dependent inflammasome activation, suggesting that intracellular CPP dissolution and calcium overload may cause this inflammation. In comparison to primary CPP, secondary CPP caused five-fold increased TNFα secretion indicating preferential stimulation of preformed cytokine secretion.

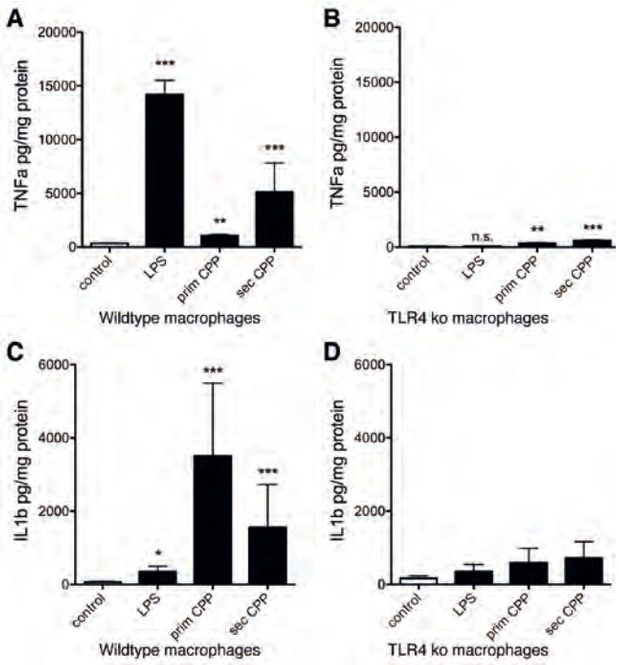

Fig. 4: CPP-induced inflammatory cytokine secretion by macrophages is TLR4 dependent.
*Wildtype and TLR4-deficient macrophages (TLR ko) where treated with LPS, primary or secondary CPP. (A, B) After 6 h stimulation, inflammatory cytokine TNFα secretion was determined in culture supernatants by ELISA. Secondary CPP caused stronger TNFα secretion than primary CPP. TLR4 ko macrophages showed 10-fold reduced TNFα secretion compared to wildtype macrophages suggesting a major contribution of TLR4 signaling in CPP-triggered TNFα secretion. Nevertheless, CPP-stimulated TLR4 ko still secreted higher amounts of TNFα compared to untreated control (prim CPP $p < 0.01$, sec CPP $p < 0.001$) suggesting a minor contribution of a TLR4-independent pathway. (C, D) After 16 h stimulation, supernatant IL-1β secreted by LPS-primed wildtype macrophages treated with primary CPP was twice as high as treated with secondary CPP Both values were significantly higher than in buffer control or with LPS treated. TLR4-deficient macrophages show a slight increase in IL-1β processing after the treatment with both types of particles. Overall, inflammatory cytokine secretion was strongly reduced in TLR4 ko. *$p < 0.05$, **$p < 0.01$, ***$p < 0.001$. Figure taken from ref [8].*

In contrast, primary CPP endocytosis did not depend on the presence of SRA, suggesting involvement of an alternative clearance pathway. CPP triggered TLR4 dependent TNF α and IL-1β secretion in cultured macrophages. Primary CPP treatment of macrophages caused low level TNFα secretion, yet strong IL-1β secretion. Calcium content-matched primary CPP caused twice more IL-1β secretion than did secondary CPP (Fig. 4 C, D), which was associated with increased calcium-dependent inflammasome activation, suggesting that intracellular CPP dissolution and calcium overload may cause this inflammation. In comparison to primary CPP, secondary CPP caused five-fold increased TNFα secretion indicating preferential stimulation of preformed cytokine secretion.

Stem Cells and Tissue Engineering

Prof. Dr. Sabine Neuß-Stein

In 2018, Sabine Neuss-Stein's group continued their research on physical and chemical cues directing stem cell behaviour [9-14]. Michaela Bienert received her PhD and moved to the Institute of Anatomy and Cell Biology as a Post-Doc. We wish her all the best for her future career. After focusing on stem cell-based bone tissue engineering using mesenchymal stem cells in the past, the group has now turned to cardiovascular tissue engineering. We secured funding by Deutsche Forschungsgemeinschaft for this work. Together with Andrij Pich (Institute of Textile and Macromolecular Chemistry) we develop fibrin-based hydrogels to direct cell answers on cardiovascular implants. In collaboration with Karolina Schickle, (Dept. of Ceramics and Refractory Materials) we test ceramic nanoparticles for stent coatings. We established hemocompatibility assays for cardiovascular implants including hemolysis and thrombogenesis. To this end we analyse blood cells (thrombocytes, monocytes, erythrocytes, Fig. 5), under static conditions as well as in flow conditions in a mechanoreactor.

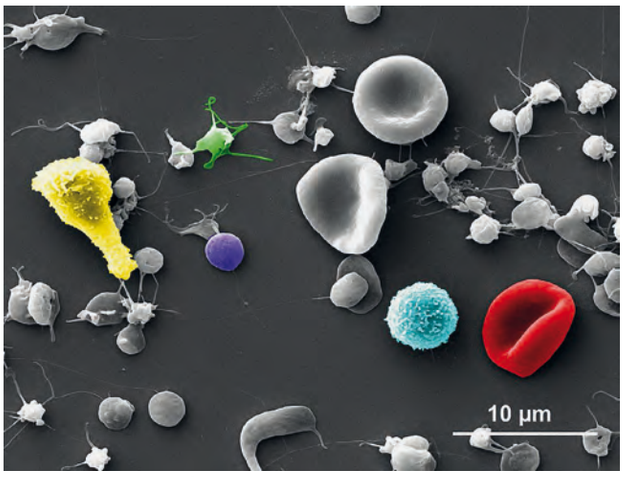

Fig. 5: SEM view of blood cells on glass slide.
Cell types are depicted by different colours: green – active thrombocyte; purple – resting thrombocyte; blue – monocyte; yellow – active monocyte; red –erythrocyte. Scale bar: 10 µm. Vuslat Parlak et al., submitted.

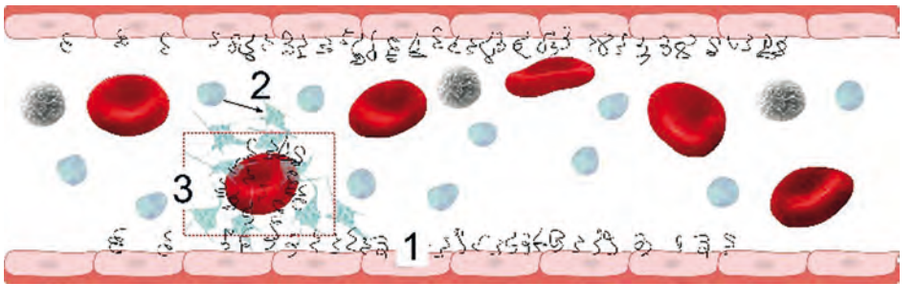

Fig. 6 (left): Start of thrombus formation within a vessel.
(1) Plasma protein deposition, (2) platelet activation, and (3) thrombus formation. Vuslat Parlak et al., submitted.

Major goals of this work are hemocompatible cardiovascular implants that prevent restenosis and allow for proper integration into the surrounding tissue while supporting endothelialization. (Fig. 6).

Development of Hemocompatibility Assays Using High-performance Ceramics

MSc Svenja Wein

Hemocompatibility is a salient feature of cardiovascular implants, e.g. stents. Platelet activation, a strong trigger of thrombosis causes stent occlusion. We studied the hemocompatibility of high strength ceramics, which can be used as nanoparticle coatings including alumina, zirconia, silicon nitride and silicon carbide. We measured the activation level of thrombocytes using platelets in static culture on the test materials. For comparison, Laminar flow conditions were also established using a bioreactor (MinuCell and MinuTissue perfusion chamber system, Munich). Platelet contact with test materials was maintained for 30 minutes at 37°C.

Figure 7 shows that all materials except Si_3N_4 and SiC (poly) activated platelets judged by the levels of CD62P and CD41a expression measured by ELISA. The number of adherent platelets, both inactive and activated, on Si_3N_4 and SiC (mono) was significantly lower than on Al_2O_3, ZrO_2, SiC (poly), glas and cupper as positive control. The positive control was generated by mechanical activation (centrifugal force) of all platelets in the sample. The highest adhesion was shown on Al_2O_3, followed by ZrO_2, SiC (poly) and glass, while SiC (mono) and Si_3N_4 showed the lowest adhesion (Fig. 7). Scanning electron microscopy (SEM) verified that more platelets adhered to samples in static conditions than in flow conditions. Platelet activation ranged from rolling to spherical and strongly adhering platelets as illustrated in Figure 8.

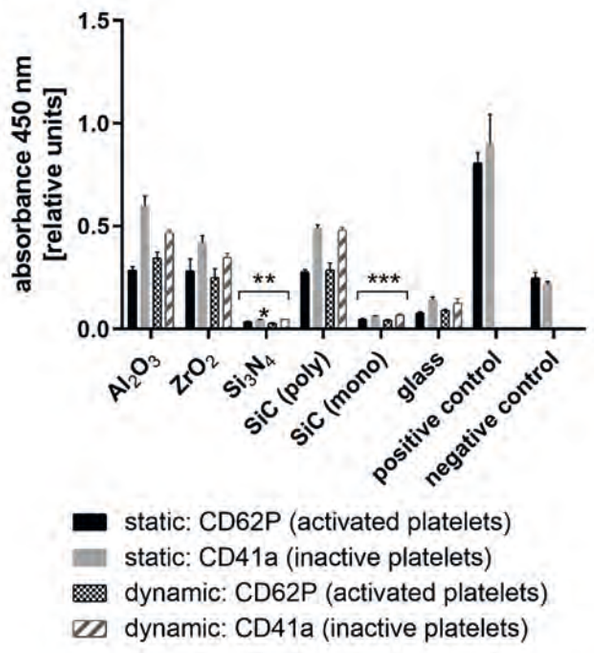

Fig. 7: Analysis of the activation stage of the thrombocytes on the ceramics determined by ELISA.
*Expression of CD62P vs. CD41a was measured for activated and non-activated platelets, respectively. Thrombocyte incubation was performed in comparison between static and dynamic conditions. There is a significant difference in activation between the amount of activated and inactivated platelets on Si_3N_4 and SiC (mono) compared to Al_2O_3, ZrO_2, SiC (poly) and glas. n=3, ***p<0.01.*

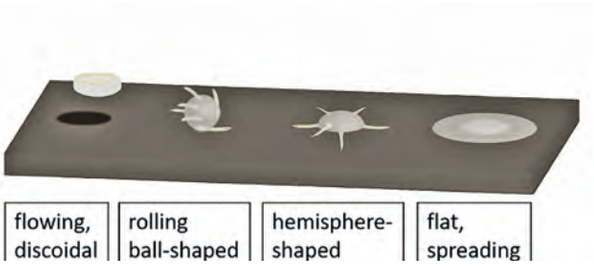

Fig. 8: Thrombocyte shape change during activation.
The shape change of platelets in response to a vascular lesion includes four stages ranging from non-activated discoidal platelets to adherent platelets. The coagulation of several adhesive thrombocytes could also be observed. A significantly lower platelet numbers could be detected under flow conditions, but there was still free material surface under static incubation conditions (Fig. 9).

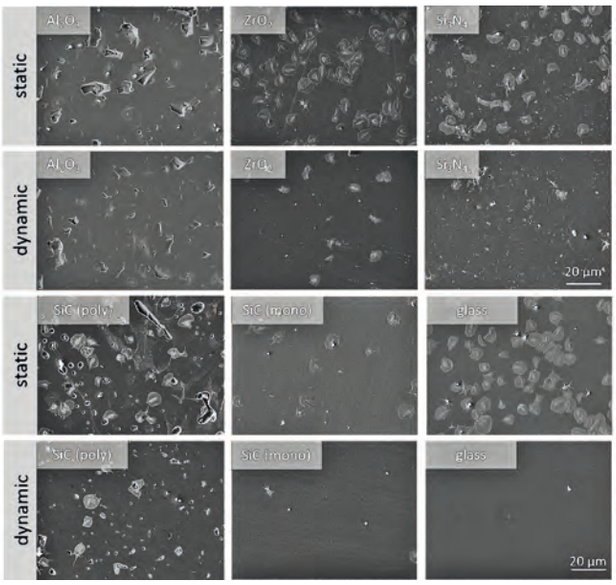

Fig. 9: Scanning electron microscopy of platelets on ceramics Al_2O_3, ZrO_2, Si_3N_4, SiC (poly), SiC (mono) and on glass.
More platelets adhered to the samples under static conditions than under flow (dynamic). Magnification: 1000x

The results of this work suggest that silicon nitride and silicon carbide in monocrystalline form should be used to coat cardiovascular implants.

Selected References

[1] Heinen, M.C., Babler, A., Weis, J., Elsas, J., Nolte, K., Kipp, M., Jahnen-Dechent, W., and Häusler, M. (2018). Fetuin-A protein distribution in mature inflamed and ischemic brain tissue. PLoS ONE 13, e0206597.

[2] Liu, A., Chen, M., Kumar, R., Stefanovic-Racic, M., O'Doherty, R.M., Ding, Y., Jahnen-Dechent, W., and Borghesi, L. (2018). Bone marrow lympho-myeloid malfunction in obesity requires precursor cell-autonomous TLR4. Nat Comms 9, 708-718.

[3] Noels, H., Boor, P., Goettsch, C., Hohl, M., Jahnen-Dechent, W., Jankowski, V., Kindermann, I., Kramann, R., Lehrke, M., Linz, D., et al. (2018). The new SFB/TRR219 Research Centre. Eur Heart J 39, 975–977.

[4] Pasch, A., Jahnen-Dechent, W., and Smith, E.R. (2018). Phosphate, Calcification in Blood, and Mineral Stress: The Physiologic Blood Mineral Buffering System and Its Association with Cardiovascular Risk. Int J Nephrol, 1, 9182078.

[5] Theek, B., Baues, M., Gremse, F., Pola, R., Pechar, M., Negwer, I., Koynov, K., Weber, B., Barz, M., Jahnen-Dechent, W., et al. (2018). Histidine-rich glycoprotein-induced vascular normalization improves EPR-mediated drug targeting to and into tumors. J Control Release 282, 25–34.

[6] Warzecha, K.T., Bartneck, M., Möckel, D., Appold, L., Ergen, C., Rawashdeh, Al, W., Gremse, F., Niemietz, P.M., Jahnen-Dechent, W., Trautwein, C., et al. (2018). Targeting and Modulation of Liver Myeloid Immune Cells by Hard-Shell Microbubbles. Adv Biosys 50, 1800002–1800011.

[7] Karmilin, K., Schmitz, C., Kuske, M., Körschgen, H., Olf, M., Meyer, K., Hildebrand, A., Felten, M., Fridrich, S., Yiallouros, I., et al. (2019). Mammalian plasma fetuin-B is a selective inhibitor of ovastacin and meprin metalloproteinases. Sci Rep 9, 546.

[8] Koeppert, S., Büscher, A., Babler, A., Ghallab, A., Buhl, E.M., Latz, E., Hengstler, J.G., Smith, E.R., and Jahnen-Dechent, W. (2018). Cellular Clearance and Biological Activity of Calciprotein Particles Depend on Their Maturation State and Crystallinity. Front Immunol 9, 1991.

[9] Ventura Ferreira M.S., Bienert M., Müller K., Rath B., Goecke T., Opländer C., Braunschweig T., Mela P., Brümmendorf T.H., Beier F., Neuss S. (2018) Comprehensive characterization of chorionic villi-derived mesenchymal stromal cells from human placenta. Stem Cell Res Ther, 9,28.

[10] Apel C., Buttler P., Salber J., Dhanasingh A., Neuss S. (2018) Differential mineralization of human dental pulp stem cells on different polymers. Biomedizinische Technik / Biomedical Engineering, 63, 261-269.

[11] Arndt P., Leistner N.D., Neuss S., Kaltbeitzel D., Brook G.A., Grosse J. (2018) Artificial urine and FBS supplemented media in cytocompatibility assays for PLGA-PEG based intravesical devices using the urothelium cell line UROtsa. Journal of Biomedical Materials Research Part B: Applied Biomaterials 106, 2140-2147.

[12] Goetzke R., Sechi A., De Laporte L., Neuss S., Wagner W. (2018) Why the impact of mechanical stimuli on stem cells remains a challenge. Cell Mol Life Sci 75, 3297-3312.

[13] Böke F., Labude N., Lauria I., Ernst S., Müller-Newen G., Neuss S., Fischer H. (2018) Biological activation of bioinert medical high performance oxide ceramics by hydrolytically stable immobilization of c(RGDyK) and BMP-2. ACS Appl Mater Interfaces. 10, 38669-38680.

[14] Wöltje M., Böbel M., Bienert M., Neuss S., Aibibu D., Cherif C. (2018) Functionalized silk fibers from transgenic silkworms for wound healing applications: Surface presentation of bioactive epidermal growth factor. J Biomed Mater Res A 106, 2643-2652.

Team 2018